Journal of Materials Chemistry

Cite this: J. Mater. Chem., 2012, 22, 7350

www.rsc.org/materials

PAPER

Incorporation of Fe^{3+} into Mg/Al layered double hydroxide framework: effects on textural properties and photocatalytic activity for H_2 generation†

Kulamani Parida,* Minarva Satpathy and Lagnamayee Mohapatra

Received 4th November 2011, Accepted 25th January 2012
DOI: 10.1039/c2jm15658j

This present work highlights the successful preparation of the ternary series of (Mg/Al + Fe)-CO_3 layered double hydroxides with a constant ratio of Mg/(Al + Fe) = 2 : 1 and their application for photocatalytic hydrogen generation from water. At Mg/(Al + Fe) = 2 : 1, the Al : Fe ratio was varied from 1 : 4 to lower the concentration of iron in the synthetic gel, in order to get samples with different amounts of iron in the brucite layers, and to find out the role of iron in photocatalytic activity. The presence of a hydrotalcite structure in the catalysts was clearly demonstrated from the powder X-ray diffraction (PXRD) pattern. The shifting of the diffraction plane d_{110} towards lower angles clearly indicated the amount of Fe^{3+} substitution in the brucite layer increases with increasing addendum (Fe^{3+}) concentration up to a certain limit and thereafter shows a decreasing trend. Further characterizations like Fourier transform infrared (FTIR), thermogravimetry (TG) and differential thermal analysis (DTA) described the formation of amorphous Fe_2O_3 upon addition of a higher amount of Fe^{3+} than the optimum amount that can be accommodated in the brucite layer. Other characterizations like UV–Vis DRS, BET surface area, transmission electron microscopy (TEM), photoluminescence spectra (PL) and X-ray photoelectron spectral studies (XPS) were performed to detect the efficiency of the catalysts towards H_2 evolution. Among all the prepared photocatalysts, LDH1(Mg/Al + Fe = 10 : 4 + 1), containing the highest amount of iron in the brucite layer, was found to be the most promising towards hydrogen evolution (301 μmol g^{-1} h^{-1}) under visible light irradiation, which was attributed to the favourable surface structure and higher crystalline nature of hydrotalcites.

Introduction

Keeping in view the impending energy crisis and the huge amount of gaseous pollutants emitted by the burning of fossil fuels for energy production, a new renewable energy source (hydrogen energy) through huge area harvesting of solar light for water splitting has been predicted. Since the pioneering discovery of Fujishima and Honda in the year 1972, TiO_2 has been considered as an effective UV active photocatalyst for H_2 evolution.[1] Detecting the inefficiency of this catalyst over $\lambda > 350$ nm, further developments on new photocatalytic materials have stepped forward.

Considering the advantages of large scale and reproducible preparation methods, layered double hydroxides (LDHs) became the challenge. Layered double hydroxides (LDHs), also known as hydrotalcite-like compounds or anionic clays are formed when a fraction of the divalent cations in a brucite-like lattice are isomorphously substituted by trivalent cations, introducing a positive charge into the layers. This extra positive charge is electrically balanced by anions present in the interlayer region, along with the water molecules. They are represented by the general formula: $[M^{II}_{(1-x)}M^{III}_{x}(OH)_2]A^{n-}_{x/n}\cdot mH_2O$, where M^{II} includes divalent metal cations like Mg^{2+}, Co^{2+}, Cu^{2+}, Ni^{2+}, Zn^{2+}, *etc.*; M^{III} may be Al^{3+}, Cr^{3+}, Ga^{3+}, Fe^{3+}, and A^{n-} might be any organic and/or inorganic anions.[2–4] Many ternary LDHs involving mixtures of different divalent and/or trivalent metal ions were also prepared.[5,6] Works on ternary hydrotalcites have extended to certain applications like catalysts in the field of organic transformation reactions and fluorescence sensitivity.[7–9]

LDHs with a cation doping capacity at the octahedral sites of the brucite layers reflected the properties of a doped semiconductor towards photocatalysis.[10] Layered double hydroxides (LDHs) have received much attention in the past decades due to their applicability as photocatalysts.[11–14] Still, the use of hydrotalcites as visible light absorbing catalysts for photocatalytic H_2 generation from water has not had many illustrations in previous research. After the prediction of Silva *et.al.*,[15] Gunjakar *et.al.*[16] also asserted the role of nanohybrids of layered Zn/Cr-LDH and layered titanate in the field of visible light induced oxygen generation. Since then, no additional studies in these essential fields, by using LDH (especially ternary LDH) as a direct photocatalyst for water reduction have been performed.

IMMT, Bhubaneswar-751 013. E-mail: paridakulamani@yahoo.com; Fax: +91-674-2581637; Tel: +91(0674) 2581636-425

† Electronic supplementary information (ESI) available. See DOI: 10.1039/c2jm15658j

The present work concerns the energy evolution under visible light irradiation, by using the ternary series of Mg/Al + Fe-CO_3 LDHs prepared through the simplest co-precipitation method. Using samples with Mg : (Al + Fe) molar ratios of 2 : 1, with the total Al + Fe = 5 and by changing the amount of two trivalent metal ions like (Mg/Al + Fe), samples such as 10 : 4 + 1 (LDH1), 10 : 3 + 2 (LDH2), 10 : 2 + 3 (LDH3), 10 : 1 + 4 (LDH4), 10 : 4.2 + 0.8 (LDH5), 10 : 4.4 + 0.6 (LDH6), 10 : 4.6 + 0.4 (LDH7), 10 : 4.8 + 0.2 (LDH8) and 10 : 5 + 0 (LDH9), were prepared, characterised and evaluated for visible light water splitting to investigate the role of the Fe^{3+} concentration in the brucite framework. A proper explanation of the photo-activity of the proposed materials is visualized in the results and discussion section. The result may provide a directional guide for the tentative study of other members of the LDH family of materials.

Experimental

Material preparation

$Mg(NO_3)_2 \cdot 6H_2O$ from S.D. Fine Chemicals, $Al(NO_3)_3 \cdot 6H_2O$ and $Fe(NO_3)_3 \cdot 9H_2O$ from Across Organics were used for the preparation of materials, as received and with no further purification. Sodium hydroxide and sodium carbonate were obtained from S.D. Fine Chemicals, India. Double distilled water was used for the preparation of the solutions.

Mixed salt solutions of $Mg(NO_3)_2 \cdot 6H_2O$, $Al(NO_3)_3 \cdot 6H_2O$, and $Fe(NO_3)_3 \cdot 9H_2O$ were prepared with Mg(II) : Al(III) + Fe(III) ratio of 2 : 1 and by changing the Al^{3+} : Fe^{3+} concentration in a proportionate way so that the Mg : (Al + Fe) ratios were 10 : 4 + 1 (LDH1), 10 : 3 + 2 (LDH2), 10 : 2 + 3 (LDH3), 10 : 1 + 4 (LDH4), 10 : 4.2 + 0.8 (LDH5), 10 : 4.4 + 0.6 (LDH6), 10 : 4.6 + 0.4 (LDH7), 10 : 4.8 + 0.2 (LDH8) and 10 : 5 + 0 (LDH9). The preparation was followed as per the literature[17] using the co-precipitation method by adding the mixed salt solutions to the prepared basic solution of NaOH + Na_2CO_3 (2 M) in a dropwise manner, maintaining a constant pH of 9.5 at room temperature with continuous stirring over 5–6 h. The resulting suspension was filtered with 0.2 μm membranes, rinsed with deionized water thoroughly to remove any excess salt and then dried at 80 °C.

Material characterisations

The samples were characterized by PXRD, FTIR, DRUV–Vis, TG–DTA, BET Surface area, TEM, PL and XPS techniques. Powder X-ray diffraction (PXRD) measurements were performed on a Rigaku D/MAX III VC diffractometer, using Cu-Kα radiation at 40 kV, a scanning rate of 5° min^{-1}, and a 2θ angle ranging from 2° to 80°. Fourier transform infrared (FTIR) spectra of the samples were recorded on a Varian FTIR spectrophotometer (FTS-800) at room temperature taking KBr as the reference in the range of 400–4000 cm^{-1}. Diffused reflectance UV–Vis (DRUV–Vis) spectra of the samples were taken with a Varian Cary IE UV–Vis spectrophotometer (model EL 96043181) equipped with a diffuse reflectance accessory in the region 200–800 nm with boric acid as reference. The TG–DTA thermograms were recorded on a Perkin-Elmer thermal analyser in the temperature range from 30 to 800 °C at a heating rate of 10 °C min^{-1} in nitrogen atmosphere. BET surface area of the samples was analyzed by the multipoint N_2 adsorption–desorption method at liquid nitrogen temperature (−196 °C) by an ASAP 2020 (Micromeritics) instrument. Prior to the analysis, the samples were degassed at 110 °C and 5 × 10^{-4} Torr for 5 h to evacuate the physically adsorbed moisture. Transmission electron microscopic (TEM) images were obtained on a Philips TECHNAI G2 operated at 200 kV, in which samples were prepared by dispersing the powdered samples in ethanol by sonication for 15 min and then drop-drying on a copper grid coated with carbon film. Photoluminescence spectra were recorded with excitation at 300 nm and measurements were performed on a Perkin-Elmer (PTP-1 Fluroscence Peltier System) L555 Fluorescence spectrophotometer. X-Ray photoelectron spectroscopy (XPS) measurements were performed on a VG Microtech Multilab ESCA 3000 spectrometer with a non-monochromatised Mg-Kα X-ray source. The energy resolution of the spectrometer was set at 0.8 eV. The binding energy correction was performed using the C 1s peak of carbon at 284.9 eV as a reference.The elemental analysis of the catalysts was determined by using atomic absorption spectroscopy (Perkin-Elmer AAS 300) with an acetylene (C_2H_2) flame.

Photocatalytic water splitting procedure

The catalytic activity and deactivation of the catalysts were studied in a batch reactor. About 0.02 g of the LDH catalyst was suspended in 20 ml of an aqueous solution containing 10 vol% of methanol. The solution was kept under constant stirring with a magnetic stirrer, preventing the settling down of particles at the bottom of the reactor. Prior to irradiation, the reaction mixture was purged with argon to eliminate the dissolved gases. A 125 W medium pressure Hg lamp (λ > 420 nm) was used as the visible light source with 1 M $NaNO_2$ solution as the UV filter. The evolved gas was collected by downward displacement of water and was analyzed on a GC-17A (Shimadzu) using a 5 Å molecular sieve column and a thermal conductivity detector (TCD). After comparing the retention time of the only peak that appeared on the chromatogram with the standard we confirmed the gas was hydrogen only.

Results and discussion

The X-ray diffraction patterns of the prepared series of ternary Mg/Al + Fe-CO_3 LDHs with different Al^{3+} : Fe^{3+} molar ratios are shown in Fig. 1. The presence of d_{003} in the particular positions of the plots illustrated the layered structure in all of the samples. However the other typical peaks encountered for the LDH structure like d_{006}, d_{009} and d_{110} are also ascribed from the plot and are indexed into a hexagonal lattice.[18] The position of the diffraction plane (003) for a 3R packing of the octahedrally arranged brucite sheets has been used to calculate the lattice parameter c as $c = 3d_{003}$, whereas the parameter a, corresponding to the average metal–metal distance in the framework was calculated from the diffraction plane (110), as $a = 2d_{110}$.[19] The lattice parameters for all the samples are given in Table 1. Due to the variation in the molar proportion of the Fe^{3+} (ionic radius = 78.5 pm in octahedral coordination) and consequent isomorphous substitution by Al^{3+} (ionic radius = 67.5 pm in octahedral coordination) in the brucite layer, the d_{110} value shifts to

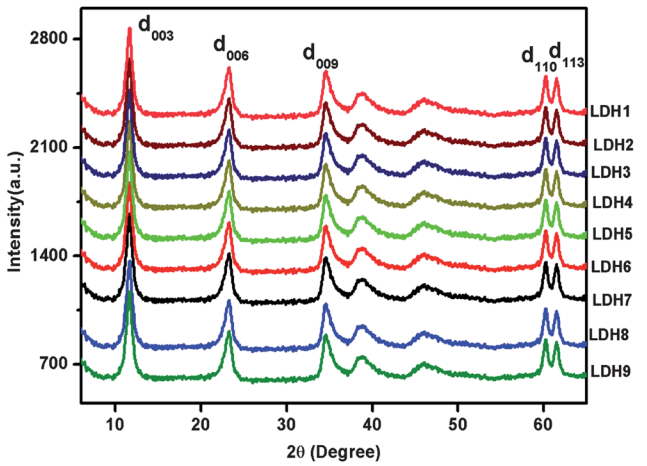

Fig. 1 X-Ray diffraction patterns of Mg/Al/Fe-CO_3 LDHs with different molar ratios.

Table 1 Cell parameters and band gap energy values of Mg/Al + Fe-CO_3 LDHs with different molar ratios

	Lattice parameters/Å[a]			
LDH	d_{003}	c	a	Band gap energy/eV[b]
LDH1	7. 6	22.69	3.09	2.8
LDH2	7.6	22.69	3.079	1.9
LDH3	7.6	22.69	3.065	1.89
LDH4	7.6	22.69	3.059	1.86
LDH5	7.6	22.69	3.08	2.9
LDH6	7.6	22.69	3.072	3.0
LDH7	7.6	22.69	3.07	3.1
LDH8	7.6	22.69	3.065	3.2
LDH9	7.6	22.69	3.06	3.5

[a] Calculated from XRD patterns. [b] UV–Vis DRS.

a slightly higher 2θ value (as shown in Fig. S1†), presenting a small steady decrease of the cell parameter a from LDH1 to LDH4 and then from LDH5 to LDH9. Slightly lower 2θ values confirmed the substitution of Fe^{3+} in the brucite layer.[20] As described in a recent paper,[21] the chemistry of LDHs containing Fe^{3+} in brucite is more complex than that of LDHs containing ions such as Al^{3+}. This has been ascribed to the solubility product of $Fe(OH)_3$ (10^{-33}) which is a large extent lower than that for $Mg(OH)_2$ (10^{-10}).[22] It is observed that, even though the hydrotalcite structure is typically assumed to be stable for $M^{2+} : M^{3+} = 2$, for Fe-LDH when the iron content is increased to a limit after which it cannot be incorporated into the LDH crystal, but it should be present in the form of amorphous iron oxides or oxohydroxides owing to the excess of unsubstituted Fe^{3+}. As a result no other crystalline phase is distinguished in the samples despite the quantitative precipitation of the salt solutions. It is reasonable to think that the amount of iron in the brucite layer increases up to a certain limit and a higher concentration of iron in the synthetic gel does not result in a higher amount of iron in the brucite layer. Evidently any other phases (iron oxide or oxohydroxide) cannot be detected from the XRD data because of the low intensity and broadened nature of their diffraction peaks, hence all excess iron has been proposed to be present as Fe_2O_3.

Another important observation found from the XRD data is that the intensities of the maxima show noticeable decreases with the increase of iron amount, drastically affecting the crystallinity of the samples.[23] Along with the increase of iron in the samples, the content of amorphous Fe_2O_3 increases and consequently the crystallinity decreases from LDH1 to LDH4. The crystallite size (D) of the LDHs was determined by employing the Scherrer formula ((eqn. 1) where λ is the wavelength of the X-ray (Cu-Kα), β is the full width at half-maximum (FWHM) of the diffraction peak, K is a shape factor (0.94), and θ is the angle of diffraction) and listed in Table 1. The crystallite size is one of the essential factors which played a vital role for the catalytic activity. The D values found in this case, have a trend of LDH4 > LDH3 > LDH2 > LDH1 and the trend of photocatalytic activity is the reverse as shown in Table S1.†

$$D = \frac{K\lambda}{\beta \cos\theta} \quad (1)$$

The FTIR spectra for the nine LDH samples are shown in Fig. 2(a) and Fig. 2(b). The FTIR spectra are expected to be of use to determine the actual bonding type in the expected compounds and to determine the substitution of Fe^{3+} in the brucite layer. The broad band centered around 3500 cm^{-1} is due to the stretching mode of hydroxyl groups, both those in the

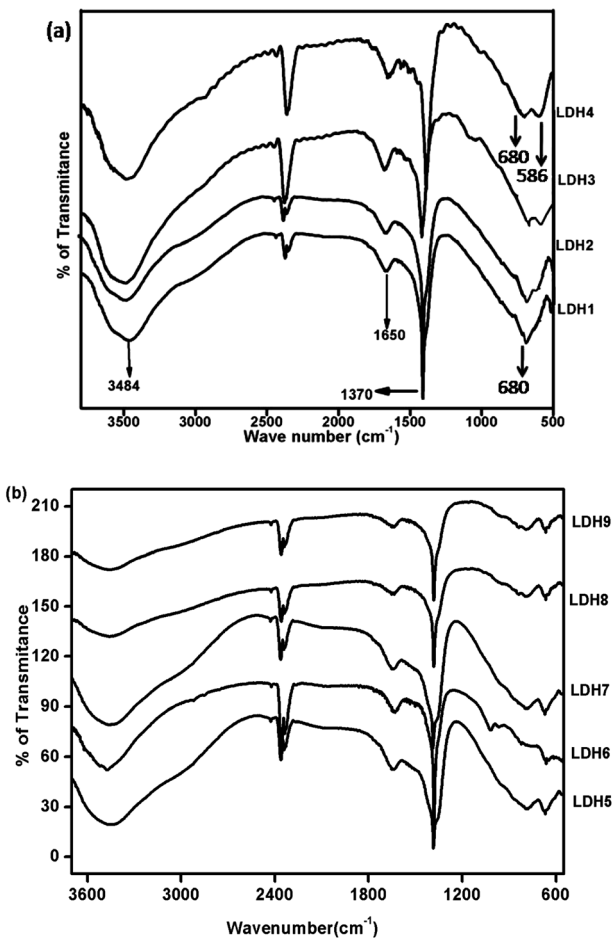

Fig. 2 FTIR spectra of (a) LDH1, LDH2, LDH3, LDH4 materials and (b) LDH5, LDH6, LDH7, LDH8, LDH9 materials.

brucite-like layers and from the interlayer water molecules of the hydrotalcite structure; the broadness of the band indicates that hydrogen bonds with a wide range of strength exist. The medium band at 1650 cm^{-1} is due to the deformation mode of water molecules;[24] the presence of different amounts of Mg^{2+}, Al^{3+} and Fe^{3+} in the brucite-like layers in the different samples would account for different relative intensities of these bands in the different spectra. The broad absorption band observed at 1370–1390 cm^{-1} is assigned to the presence of carbonate ions.[25] The bands below 1000 cm^{-1} are due to M–O vibration modes. Bands observed near lower wave numbers (580–690 cm^{-1}) might be attributed to the stretching vibrations of M–O, M–O–M, and O–M–O bands in the layer as well as the asymmetric stretching frequencies of interlayer carbonates.[26] LDH1 exhibits only one peak at 680 cm^{-1} which is characteristic of a crystalline and phase pure hydrotalcite. This single peak is explained on the basis of the isomorphous substitution of Al^{3+} by Fe^{3+}, leading to the change in the element in the brucite layer. However, as the amount of Fe^{3+} ion increases in the LDHs, the single peak changes into two peaks in the range of 580–690 cm^{-1}. The characteristic absorption band at 586 cm^{-1} for LDH4 powder is assigned to α-Fe_2O_3.[27]

For the detection of the photocatalytic activity, investigation of the optical absorption behaviour of the catalyst is indispensable. The UV–Vis diffuse reflectance spectra of the as prepared samples are shown in Fig. 3 (a) and 3(b). Mg/Al-CO_3 LDH (2 : 1) is clearly an UV-active species. The red shift of the absorption edges increases in the order: LDH9 < LDH8 < LDH7 < LDH6 < LDH5 < LDH1 < LDH2 < LDH3 < LDH4 and is ascribed to the increase in concentration of Fe^{3+}.[28] Absorbance in the visible region for all the prepared LDHs proves that all of them are capable of absorbing photons within the visible range except LDH7, LDH8 and LDH9 which are UV active. Conversely all of them cannot be used as catalysts for water splitting. The band gap energy values were calculated by eqn (2) and are given in Table 1.

$$E_g(\text{eV}) = \frac{1240}{\lambda(\text{nm})} \quad (2)$$

The order of photoactivity towards H_2 evolution does not follow the same trend as the absorption wavelength due to the formation of amorphous iron oxide on the surface. The band edge potentials for ($200 < \lambda < 300$ nm) can be explained on the basis of charge transfer (LMCT) excitations occurring in the MO_6 octahedra of layered structure.[29] However the absorbance above 400 nm in the case of LDH1 is due to the d–d transition of Fe^{3+}. On the other hand, the red shift of absorption wavelength $\lambda > 600$ nm in LDH2 to LDH4 is due to the interband d–d transitions of the Fe_2O_3 particles formed on the surface of hydrotalcite phase.[30]

The TG–DTA plots detecting the measure of the weight loss occurring in the LDHs due to temperature variation are shown in Fig. 4. The TGA plots (Fig. 4(a)) for all of them except LDH4, reveal the two step weight loss process, generally observed in case of normal hydrotalcites. In all the three types of hydrotalcites excluding LDH4, the first weight loss step (16%) up to 200–240 °C is due to the removal of the physisorbed and loosely bonded interlayer water molecules. The second weight loss (41%) around 435–450 °C is attributed to the removal of water by dehydroxylation of hydroxyl groups in the brucite-layers and also corresponds to the decarboxylaton of interlayer CO_3^{2-} anions.[31] In case of LDH4, the first step of weight loss (11%) begins at 156 °C which indicated the surface adsorbed water molecules and the loss of hydroxyls (21%) observed at 315 °C. Further weight losses (33%, 38%) seen at 550 °C and 770 °C may be due to the higher weight losses due to the formation of Fe_2O_3 as the hydrotalcite phase does not exist beyond a temperature of 500 °C.[32] Differential thermal analysis curves for the prepared samples, shown in Fig. 4(b) contribute peaks to the endothermic weight loss. The first endothermic peak at 160 °C is associated with the removal of interlayer water molecules and the second peaks at 330 °C are due to removal of layer hydroxyls and interlayer carbonates. The intensity of the second peak drastically decreases as the Fe content increases in the samples.[33]

The nitrogen adsorption–desorption studies were performed for further characterizing these samples and corresponding isotherms are shown in Fig. S2.† All of them followed a type IV isotherm with a H3 hysteresis loop indicating aggregation of plate-like particles with slit-like pores according to the IUPAC classification. The BET-surface area values of the samples LDH1 to LDH4 were given in Table S1.† The specific surface area was found to increase from LDH1 to LDH4 which can be attributed to the deposition of amorphous Fe_2O_3 aggregates on the LDH surface with the increased iron amount. As the formation of the Fe_2O_3 phase increases so the surface area increases from LDH1 to LDH4.[34]

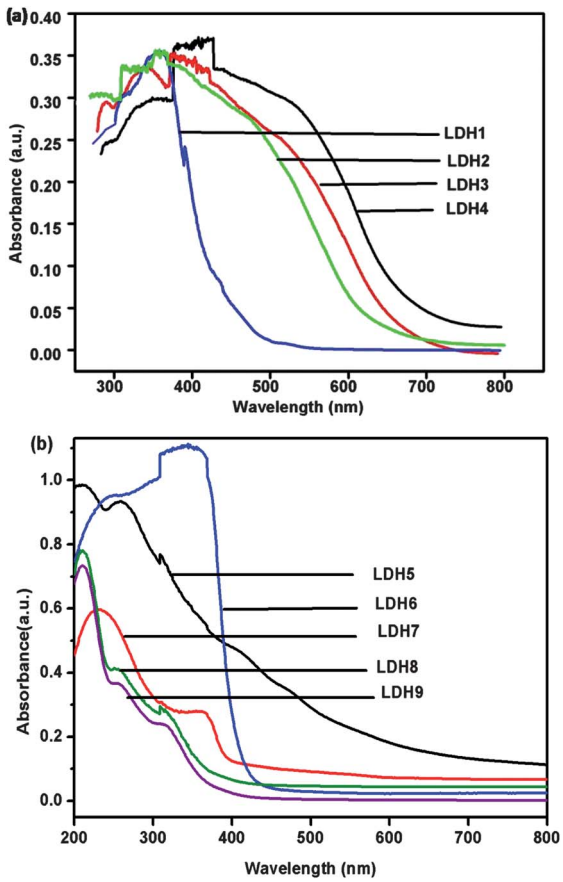

Fig. 3 UV–Vis diffuse reflectance spectra of (a) LDH1, LDH2, LDH3 and LDH4 materials and (b) LDH5, LDH6, LDH7, LDH8, and LDH9 materials.

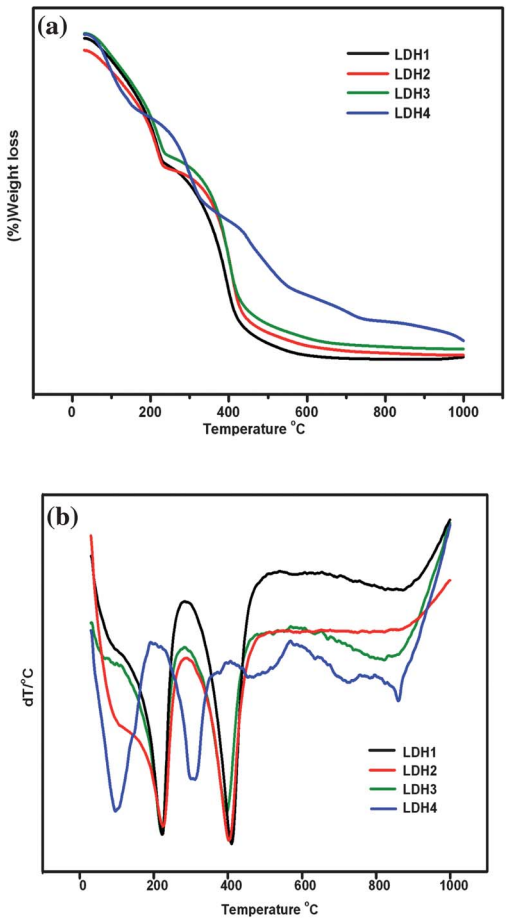

Fig. 4 (a) TG curves of Mg/Al/Fe-CO_3 LDHs with different molar ratios. (b) DTA curves of Mg/Al/Fe-CO_3 LDHs with different molar ratios.

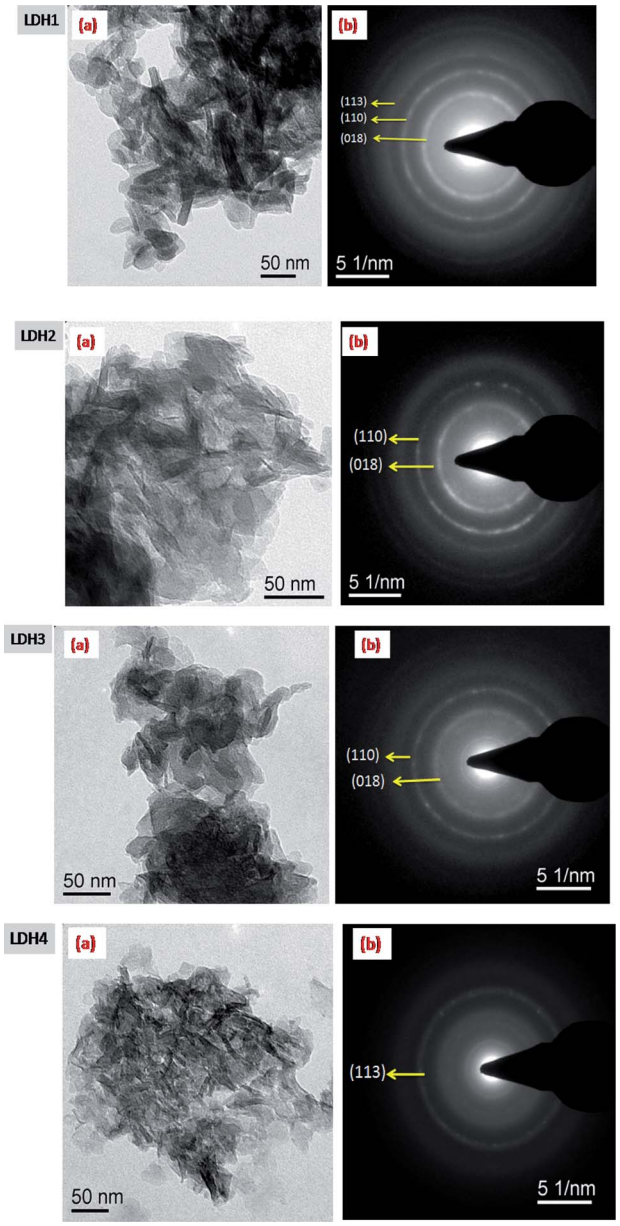

Fig. 5 (a) TEM images (b) SAED of all as prepared Mg/Al/Fe-CO_3 LDHs.

Fig. 5 shows the transmission electron microscopic images of the hydrotalcite samples. They are small and irregular flakes with well dispersed particles for LDH1. The particle size decreases upon the incorporation of iron into the brucite-like layers. The selected area electron diffraction (SAED) pattern taken from these nano-crystalline particles shown in the figures clearly reveals the presence of concentric diffraction rings of pure LDH phases.[35,36] The decrease in crystallinity from LDH1 to LDH4 can be clearly detected from the SAED patterns with the disappearance of a number of concentric rings, from which we can also predict the growth of the amorphous Fe_2O_3 phase.

Effective inhibition of electron–hole pair recombination is very much essential for an efficient photocatalyst, which is based on the surface charge transfer phenomenon. Photoluminescence emission results from the recombination of excited electrons and holes, therefore lower PL intensity indicates lower rates of recombination and fruitful photoactivity. As can be visualised from Fig. 6, a PL study of the various LDH photocatalysts with visible light at room temperature predicted a maximum recombination rate for LDH4 due to a larger amount of amorphous iron oxide formation. On the other hand, LDH1 showed a lower intense emission suggesting the lowest recombination rate and highest activity towards visible light driven H_2 evolution. The decreased recombination is mainly due to the favoured substitution of Fe^{3+} at the brucite framework. The presence of iron favours the migration of photoproduced electrons to the conduction band and Fe^{3+} ions trap electrons, thus improving the electron hole separation.[37] The elemental analysis of all catalysts are given in Table S1.†

The XPS survey scans were used to identify the surface properties of the iron substituted LDH samples. XPS spectra of the LDH1 substrate are shown in Fig. S3† suggesting their existence in hydroxide form with carbonate in the interlayer space. In the present study, the main peak of C 1s is observed at a B.E. value of 285.0 eV and another one at 289.0 eV clearly suggests the presence of carbonate anions in the structure of LDH. Two values, 531.5 eV and 532.5 eV, for O 1s were observed. The first one, with a very low intensity is attributed to oxygen bonded to carbon species in the interlayer position of

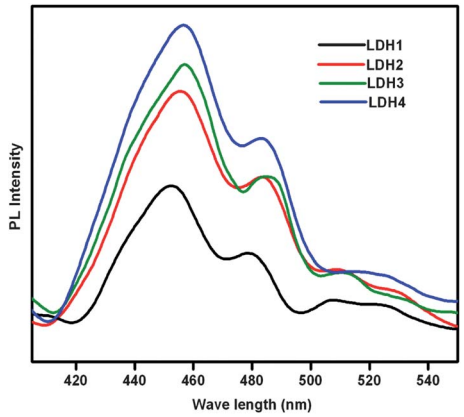

Fig. 6 Photoluminescence spectra of Mg/Al/Fe-CO_3 LDHs with different molar ratios.

LDH, whereas the high intensity second peak corresponds to the oxygen species in hydroxide form in the LDH structure. The Mg (2p) value is found to be at 50.0 eV indicating that the Mg^{2+} is present in the hydroxide form. The B.E of Al (2p) is observed at 73.6 eV, confirming the octahedral Al^{3+} is present in the brucite layer of LDH. The presence of Fe $2p_{3/2}$ core level spectra at 712.5 eV in the LDH sample showed unambiguously the presence of Fe^{3+} in the solids.[38]

Photocatalytic activity test

In the present work, photocatalytic H_2 production activities of the prepared LDHs were evaluated under visible-light irradiation using methanol as a sacrificial reagent. Control experiments (without photocatalysts) indicated that no appreciable hydrogen production was detected in the absence of either irradiation or photocatalyst, suggesting that hydrogen was produced by photocatalytic reactions. Fig. 7(a) shows the H_2 evolution from water with different LDH photocatalyst suspensions under visible light irradiation without the loading of any co-catalyst. The rate of H_2 evolution in LDH1 was about 301 μmol g^{-1} h^{-1}, higher than LDH2 (493 μmol g^{-1} h^{-1}), LDH3 (332 μmol g^{-1} h^{-1}), LDH4 (265 μmol g^{-1} h^{-1}), LDH5 (68 μmol g^{-1} h^{-1}), LDH6 (65 μmol g^{-1} h^{-1}), LDH7 (29 μmol g^{-1} h^{-1}), LDH8 (11 μmol g^{-1} h^{-1}), and LDH9 (6 μmol g^{-1} h^{-1}) and continued for 3 h under ambient conditions from which the abilities of different catalysts were detected. Fig. 7(b) showed that H_2 production stopped when the light was turned off (dark region) and similar hydrogen productions were observed in three repeated runs. This indicates that water splitting in aqueous methanol solution on these photocatalysts can be made repeatedly without deactivation.

In order to determine the effect of concentration of photocatalysts on hydrogen evolution for LDH1, experiments were performed by varying the material concentrations from 0.2 to 1.5 g L^{-1}. Fig. S4† presents the influence of the photocatalyst doses on the initial rate of hydrogen generation where a concentration of 1 g L^{-1} was found to give the highest photocatalytic activity for the same system under these conditions. With a high dose of photocatalyst, there will be a decrease in the penetration of light due to an increase in turbidity of the suspension and hence the photoactivated volume of the suspension decreases. Thus it can

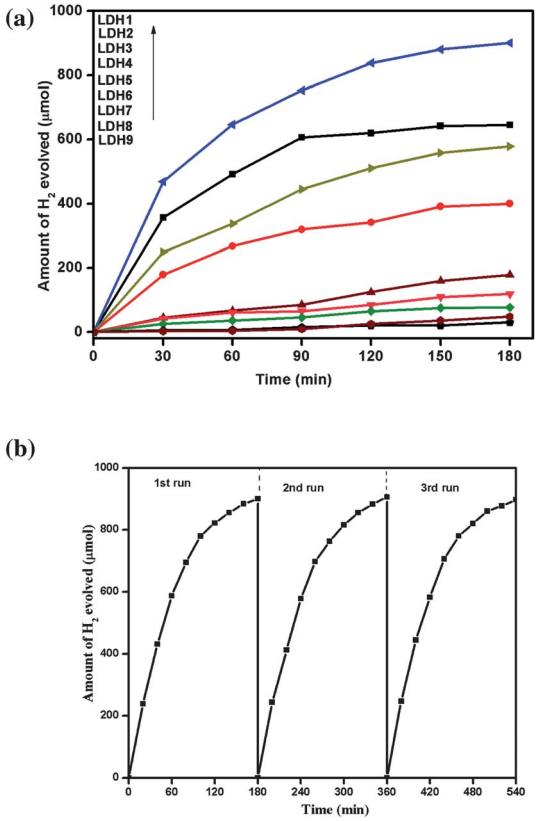

Fig. 7 (a) Temporal changes in the amount of hydrogen evolved (μmol) with different LDHs during irradiation. (b) Volume of hydrogen evolved in three consecutive cycles run every 180 min.

be concluded that a higher dose of catalyst may not be good for photocatalysis.

The H_2 production rate is significantly greater in LDH1 than for the other three LDH photocatalysts. This is attributed to various factors. Mg/Al-CO_3 LDH is an UV-active photocatalyst and is inactive towards visible light effective water decomposition. However, the rigorous substitution of Fe^{3+} into the framework makes it visible light active and results in a consequent decrease of the band gap energy due to the formation of $Fe(OH)_6$ octahedral units. On the other hand from LDH1 to LDH4 we cannot find a subsequent trend of activity. For samples LDH2, LDH3 and LDH4, we found a decreasing trend for H_2 evolution compared to LDH1. So, in this case the temporal changes of the amount of evolved H_2 with variation in samples cannot be explained on the basis of the varying band gap energy and surface area values. In order to explain the higher activity of LDH1, the replacement of Fe^{3+} at an appropriate position in the brucite framework is essential. LDHs act as doped semiconductors and Fe^{3+} has been shown to be a more effective dopant for enhancing the photocatalytic activity of Mg/Al-CO_3LDH by shifting the light absorbance towards visible range. By increasing the amount of iron content in the sample, growth of amorphous iron oxide phases occurs, avoiding substitution at brucite sites, which helps in absorbing a maximum amount of the visible light and increasing the surface area as well as increasing the recombination of the photoinduced e^-s and h^+s, thereby decreasing the photocatalytic activity. Another important factor

is crystallite size. LDH1 has a smaller crystallite size (as detected from the XRD pattern) than others. Also the hydroxide groups present in the LDH surface capture the photoinduced holes (h^+), consequently preventing the recombination of the h^+s and e^-s, as a result, improving the photocatalytic activity.

Fe substituted LDH had a significant influence on the photocatalytic activity. For LDH4 (greater amount of iron content as amorphous iron oxides), a relatively low photocatalytic H_2 production rate was observed, as expected, due to the rapid recombination of conduction band (CB) electrons and valence band (VB) holes as evidenced from the PL study. Due to the presence of an optimum amount of Fe^{3+} in the experimental solution, the activity of LDH1 is maximum towards hydrogen evolution, since the amount of iron oxide was the lowest, and all of the iron content occurred as cations doped into the brucite sheet to enhance the hydrogen evolution.

An illustration mechanism was proposed to better understand the photocatalytic activities of LDH1 in the presence of a sacrificial reagent (eqn (3)–(9)). LDHs are constituted of sheets of edge-sharing $M(III)O_6$ octahedral units. Upon exposure to visible light irradiation with an energy equal to or greater than the band gap energy, the electron from the valence band of LDH1 (O 2p orbital) was excited to the conduction band of Fe^{3+} (3d orbital) and the H^+ accepts the electrons in the conduction band, producing hydrogen gas, as shown below eqn (3)–(5). Aqueous methanol was used here as a hole scavenger.When the LDH suspension was exposed to visible radiation in the presence of 10% aqueous methanol, there is a possibility that methanol molecules can be oxidised to HCHO, HCOOH, CO_2, H_2 and also CH_4. But chromatographic analysis of the produced gases revealed that CO_2 is the only byproduct that is also present in a very minor amount. It has also been found that a limited amount of hydrogen gas evolved from the methanol. So, it is reasonable to confirm that H_2 evolved from the photocatalytic process over LDH1 and the sacrificial reagent can protect the photocatalysts from photocorrosion by providing sacrificial electron donors to consume the photogenerated holes.[39–43]

$$Zn/Al + Fe\ LDH(FEO_6) \xrightarrow{h\nu,\ Catalyst} h^+ + e^- \quad (3)$$

$$2H_2O \rightarrow 2H^+ + 2OH^- \quad (4)$$

$$2e^-_{CB} + 2H^+ \rightarrow H_2 \quad (5)$$

$$CH_3OH \xrightarrow{h\nu,\ Catalyst} HCHO + H_2 \quad (6)$$

$$HCHO + H_2O \xrightarrow{h\nu,\ Catalyst} HCO_2H + H_2 \quad (7)$$

$$HCO_2H \xrightarrow{h\nu,Catalyst} CO_2 + H_2 \quad (8)$$

$$CO_2 + H_2O \xrightarrow{h\nu,\ Catalyst} CH_4 \quad (9)$$

Conclusions

Mg/(Al + Fe)-CO_3 LDH (Fe-doped Mg/Al-CO_3 LDH) materials were prepared by a simple co-precipitation method and thoroughly characterized by structural, spectroscopic, textural, optical and microscopic methods with powder X-ray diffraction (PXRD), Fourier transform infrared (FTIR), X-ray photoelectron spectral studies (XPS), thermogravimety (TG) and differential thermal analysis (DTA), UV–Vis DRS, BET surface area, photoluminescence spectra (PL) and transmission electron microscopy (TEM) methods. This may be the first report of the use of Fe^{3+} as a dopant for Mg/Al-CO_3 LDH which has all the aspects needed to shift the absorption towards the visible light region, utilising the ternary hydrotalcite as a relevant photocatalyst for water decomposition. By studying the visible-light photocatalytic activity of all the LDH samples with different proportions of doped Fe^{3+}, the following conclusions can be drawn: (i) LDH1 with a higher content of Fe^{3+} in the brucite framework was well crystallised, possessed abundant surface water and hydroxyl groups, and hence high photocatalytic efficiency in the visible range; (ii) the concentration of the Fe^{3+} salt solution has a significant effect on the nucleation and formation of the LDH-phase. Excess iron in the synthetic gel, due to its larger ionic radius compared to Al^{3+} may form amorphous Fe_2O_3 without substituting in the hydrotalcite brucite stalks. This amorphous iron phase accelerates the recombination rate of the photogenerated electrons and holes causing a decrease in H_2 evolution. of visible light irradiated water splitting, LDH1 possessed promising characteristics for exploitation as a futuristic material.

Acknowledgements

The authors are thankful to Prof. B. K. Mishra, Director, Institute of Minerals & Materials Technology (IMMT), Bhubaneswar, for his constant encouragement and kind permission to publish this paper.

Notes and references

1 A. Fujishima and K. Honda, *Nature*, 1972, **238**, 37.
2 O. Saber and H. Tagaya, *J. Inclusion Phenom. Macrocyclic Chem.*, 2003, **45**, 109.
3 D. Carriazo, C. Martın, V. Rives, A. Popescu, B. Cojocaru, I. Mandache and V. I. Parvulescu, *Microporous Mesoporous Mater.*, 2006, **95**, 39.
4 P. Nalawade, B. Aware, V. J. Kadam and R. S. Hirlekar, *J. Sci. Ind. Res.*, 2009, **68**, 267–272.
5 J. Carpentier, S. Siffert and J. F. Lamonier, *J. Porous Mater.*, 2007, **14**, 103.
6 V. Rives, A. Dubeyb and S. Kannanb, *Phys. Chem. Chem. Phys.*, 2001, **3**, 4826.
7 A. Alejandre, F. Medina, X. Rodriguez, P. Salagre, Y. Cesteros and J. E. Sueiras, *Appl. Catal., B*, 2001, **30**, 195.
8 S. Kannan, A. Dubey and H. Knozinger, *J. Catal.*, 2005, **231**, 381.
9 Y. Chen, S. Zhou, F. Li, J. Wei, Y. Dai and Y. Chen, *J. Fluoresc.*, 2011, **21**, 1677.
10 B. Schwenzer, J. R. Neilson, K. Sivula, C. Woo, J. M. J. Frechet and D. E. Morse, *Thin Solid Films*, 2009, **517**, 5722.
11 Y. Lee, J. H. Choi, H. J. Jeon, K. M. Choi, J. W. Lee and J. K. Kang, *Energy Environ. Sci.*, 2011, **4**, 914.
12 A. Mantilla, F. Tzompantzi and J. L. Fernandez, *et.al.*, *Catal. Today*, 2009, **148**, 119.
13 J. Orthman, H. Y. Zhu and G. Q. Lu, *Sep. Purif. Technol.*, 2003, **31**, 53.
14 G. Centi and S. Perathoner, *Microporous Mesoporous Mater.*, 2008, **107**, 3–15.
15 C. Silva, Y. Bouizi, V. Fornes and H. Garcıa, *J. Am. Chem. Soc.*, 2009, **131**, 13833.
16 J. L. Gunjakar, T. W. Kim, H. N. Kim, I. Y. Kim and S. Hwang, *J. Am. Chem. Soc.*, 2011, **133**, 14998.

17 S. Kannan, A. Dubey and H. Knozinger, *J. Catal.*, 2005, **231**, 381.
18 Gabriela Carja, Ryuichi Nakamura and Hiroo Niiyama, *Appl. Catal., A*, 2002, **236**, 91.
19 G. Wu, L. Wang, D. G. Evans and X. Duan, *Eur. J. Inorg. Chem.*, 2006, 3185–3196, DOI: 10.1002/ejic.200600203.
20 C. Jiao, Zheng-Zhou Wang, Xi-Lei Chen and Yuan- Hu, *J. Appl. Polym. Sci.*, 2007, **107**, 2626.
21 G. V. Manohara, S. V. Prasanna and P. Vishnu Kamath, *Eur. J. Inorg. Chem.*, 2011, 2624–2630, DOI: 10.1002/ejic.201100104.
22 D. Dobos, *Electrochemical Data a Handbook for Electrochemist's in Industry and Universities*, Elsevier, Amsterdam, 1975.
23 J. M. Fernandez, M. A. Ulibarri, F. M. Labajos and V. Rives, *J. Mater. Chem.*, 1998, **8**, 2507.
24 M. R. Kang, H. M. Lim, S. C. Lee, S. Lee and K. J. Kim, *J. Mater. Online*, 2005, **1**, 3.
25 R. M. Queiroz, L. H. O. Pires, R. C. P. de Souza, J. R. Zamian, A. G. de Souza, G. N. da Rocha Filho and C. E. F. da Costa, *J. Therm. Anal. Calorim.*, 2009, **97**, 163.
26 Y. Chuang, Y. Tzou, M. K. Wang, C. H. Liu and P. N. Chiang, *Ind. Eng. Chem. Res.*, 2008, **47**, 3813.
27 M. Mahmoudi, A. Simchi, M. Imani and U. O. Hafeli, *J. Phys. Chem. C*, 2009, **113**, 8124.
28 J. Torrent and V. Barron, Encyclopedia of Surface and Colloid Science, 2002, pp. 1438–1446.
29 D. A. Skoog, D. M. West, F. J. Holler, *Fundamentals of Analytical Chemistry*, 7th Edition, Thomson Learning, Inc, USA, 1996.
30 S. S. Shinde, R. A. Bansode, C. H. Bhosale and K. Y. Rajpure, *J. Semicond.*, 2011, **32**, 013001.
31 R. Chitrakar, S. Tezuka, A. Sonoda, K. Sakane and T. HirotsuInd, *Ind. Eng. Chem. Res.*, 2008, **47**, 4905.
32 V. Choudhary, R. Jha and P. A Choudhari, *J. Chem. Sci.*, 2005, **117**, 635.
33 J. Carpentier, S. Siffert, J. F. Lamonier, H. Laversin and A. Aboukas, *J. Porous Mater.*, 2007, **14**, 103.
34 S. Kakuta and T. Abe, *J. Mater. Sci.*, 2009, **44**, 2890.
35 G. Carja, A. Nakajima, S. Dranca, C. Dranca and K. Okada, *J. Phys. Chem. C*, 2010, **114**, 14722.
36 A. H. Padmasri, A. Venugopal, V. Durga Kumari, K. S. Rama Rao and P. Kanta Rao, *J. Mol. Catal. A: Chem.*, 2002, **188**, 255.
37 S. H. Othman, S. A. Rashid, T. I. M. Ghazi and N. Abdullah, *J. Nanomater.*, 2011, Article ID 571601.
38 M. P. Nikiforov, M. V. Chernysheva, A. V. Lukashin, A. A. Vertegel, Yu. V. Maksimov, S. V. Novichikhin, I. P. Suzdalev and A. Yu. D. Tretyakov, *Dokl. Chem.*, 2003, **391**, 173.
39 O. Rosseler, M. V. Shankar, M. K. Du, L. Schmidlin, N. Keller and V. Keller, *J. Catal.*, 2010, **269**, 179.
40 H. Husin, W. Su, H. Chen, C. Pan, S. Chang, J. Rick, W. Chuang, H. Sheuc and B. Hwang, *Green Chem.*, 2011, **13**, 1745.
41 T. Puangpetcha, T. Sreethawong, S. Yoshikawac and S. Chavadej, *J. Mol. Catal. A: Chem.*, 2009, **312**, 97.
42 R. Dholam, N. Patel, M. Adami and A. Miotello, *Int. J. Hydrogen Energy*, 2009, **34**, 5337.
43 K. M. Parida, S. Martha, D. P. Das and N. Biswal, *J. Mater. Chem.*, 2010, **20**, 7144.